The Journal of Physiology

Fluorescence recovery after photobleaching reveals regulation and distribution of connexin36 gap junction coupling within mouse islets of Langerhans

Nikki L. Farnsworth[1], Alireza Hemmati[2], Marina Pozzoli[2] and Richard K. P. Benninger[1,2]

[1] Barbara Davis Center for Childhood Diabetes, University of Colorado, Aurora, CO, USA
[2] Department of Bioengineering, University of Colorado, Aurora, CO, USA

Key points

- Gap junctions provide electrical coupling that is critical to the function of pancreatic islets. Disruptions to connexin36 (Cx36) have been suggested to occur in diabetes.
- No accurate and non-invasive technique has yet been established to quantify changes in Cx36 gap junction coupling in the intact islet.
- This study developed fluorescence recovery after photobleaching (FRAP) as a non-invasive technique for quantifying Cx36 gap junction coupling in living islets.
- The study identified treatments that modulate gap junction coupling, confirmed that the cellular distribution of coupling throughout the islet is highly heterogeneous and confirmed that α cells and β cells do not form functional Cx36 gap junctions.
- This technique will enable future studies to examine the regulation of Cx36 gap junction coupling and its disruption in diabetes, and to uncover potential novel therapeutic targets associated with gap junction coupling.

Abstract The pancreatic islets are central to the maintenance of glucose homeostasis through insulin secretion. Glucose-stimulated insulin secretion is tightly linked to electrical activity in β cells within the islet. Gap junctions, composed of connexin36 (Cx36), form intercellular channels between β cells, synchronizing electrical activity and insulin secretion. Loss of gap junction coupling leads to altered insulin secretion dynamics and disrupted glucose homeostasis. Gap junction coupling is known to be disrupted in mouse models of pre-diabetes. Although approaches to measure gap junction coupling have been devised, they either lack cell specificity, suitable quantification of coupling or spatial resolution, or are invasive. The purpose of this study was to develop fluorescence recovery after photobleaching (FRAP) as a technique to accurately and robustly measure gap junction coupling in the islet. The cationic dye Rhodamine 123 was used with FRAP to quantify dye diffusion between islet β cells as a measure of Cx36 gap junction coupling. Measurements in islets with reduced Cx36 verified the accuracy of this technique in distinguishing between distinct levels of gap junction coupling. Analysis of individual cells revealed that the distribution of coupling across the islet is highly heterogeneous. Analysis of several modulators of gap junction coupling revealed glucose- and cAMP-dependent modulation of gap junction coupling in islets. Finally, FRAP was used to determine cell population specific coupling, where no functional gap junction coupling was observed between α cells and β cells in the islet. The results of this study show FRAP to be a robust technique which provides the cellular resolution to quantify the distribution and regulation of Cx36 gap junction coupling in specific cell populations within the islet. Future studies utilizing this technique may elucidate the role of

gap junction coupling in the progression of diabetes and identify mechanisms of gap junction regulation for potential therapies.

Abbreviations α-GA, 18-α-glycyrrhetinic acid; C57BL/6, C57BL/6NHsd; Ca^{2+}, free calcium; $[Ca^{2+}]_i$, intracellular free calcium; $cAMP_i$, intracellular cyclic adenosine monophosphate; Cx36, connexin36; FRAP, fluorescence recovery after photobleaching; HBSS, Hank's balanced salt solution; IBMX, 3-isobutyl-1-methylxanthine; Rh123, Rhodamine 123; RoI, region of interest.

Introduction

The pancreatic islets of Langerhans are central to the maintenance of blood glucose homeostasis. Insulin secretion from β cells is initiated by metabolic and electrical events, in which glucose-stimulated electrical activity regulates insulin secretion. Gap junctions, composed of connexin36 (Cx36), form intercellular channels that couple cells within the islet, allowing for the passage of cationic molecules such as calcium (Ca^{2+}) (Charpentier *et al.* 2007; Bukauskas, 2012). Under glucose stimulation, Cx36 gap junctions coordinate intracellular free-calcium ($[Ca^{2+}]_i$) oscillations (Benninger *et al.* 2008), resulting in the coordination of insulin secretion across the islet. In Cx36 knockout mice, loss of coordination of $[Ca^{2+}]_i$ oscillations, reduced first-phase insulin release, loss of pulsatile second-phase insulin release, and glucose intolerance are observed (Ravier *et al.* 2005; Spier *et al.* 2007; Head *et al.* 2012). These changes to insulin release dynamics are similar to those seen in humans with type 2 diabetes and those with obesity (O'Rahilly *et al.* 1988; Menge *et al.* 2011). This, along with studies which have shown Cx36 disruption in a mouse model of pre-diabetes (Carvalho *et al.* 2012), suggest that changes in Cx36 gap junction coupling may play a role in the islet dysfunction underlying diabetes, as reviewed in Perez-Armendariz (2013) and Farnsworth & Benninger (2014).

Whereas the role of Cx36 gap junction coupling in physiological insulin release has been well established, the distribution of functional coupling between β cells and other cell types in the islet is largely unknown. Other islet cell types, such as α cells and δ cells, are known to be able to affect the regulation of insulin secretion. Although this may occur through paracrine communication of secreted hormones such as glucagon or somatostatin (Sorensen *et al.* 2006; Hauge-Evans *et al.* 2009), the presence or absence of gap junction coupling between β cells and other islet cell types has not been established. Many studies have found that, in mice and humans, β cells are functionally heterogeneous and that glucose responsiveness, electrical dynamics and insulin secretion are highly variable across an islet (Pipeleers, 1992; Benninger *et al.* 2008; Wojtusciszyn *et al.* 2008).

Recent studies have strongly implied the presence of heterogeneity in coupling (Stozer *et al.* 2013; Hraha *et al.* 2014) and that mathematical models of the islet require heterogeneous gap junction conductance to fully describe spatiotemporal $[Ca^{2+}]_i$ and electrical oscillations underlying insulin release (Benninger *et al.* 2008; Goel & Mehta, 2013). To our knowledge, no studies have directly quantified the spatial distribution of Cx36 gap junction coupling across the intact islet with cellular resolution. The lack of characterization of Cx36 gap junction coupling in the islet is largely attributable to the lack of techniques available to accurately determine functional coupling and conductance across an intact islet, with spatial and temporal resolution.

A number of methods have been employed to measure gap junction coupling in various tissues (Abbaci *et al.* 2008). Within the islet, some studies have used measurements of electrical coupling as indicators of Cx36 gap junction conductance. These include perforated-patch measurements of total coupling conductance to quantify total Cx36 gap junction conductance (Benninger *et al.* 2008). However, this technique can measure conductance in only one cell at a time and only in cells on the surface of an islet, which makes it difficult to spatially resolve coupling. Similarly, dual patch clamp experiments have been used with β cell pairs (Moreno *et al.* 2005), although the results may not be representative of coupling in an intact islet. The anionic dye Lucifer yellow has been used in dye injection in the islet (Ravier *et al.* 2005; Bavamian *et al.* 2012); however, as Cx36 gap junctions are cationic-specific, measurements with Lucifer yellow do not show strong coupling (Charpentier *et al.* 2007). The cationic DNA-binding dye ethidium bromide has been used with micro-injection to measure Cx36 gap junction coupling, but this still only gives an average assessment of coupling across the whole intact islet (Carvalho *et al.* 2010). In fibroblasts, local activation of a molecular fluorescent probe (LAMP) has been used to study gap junction coupling with cellular resolution (Dakin *et al.* 2005). However, this technique uses an anionic dye and is therefore not suitable for Cx36 gap junctions in the islet.

Fluorescence recovery after photobleaching (FRAP) has been used to dynamically measure functional gap junction

conductance in astrocytes (Lee *et al.* 2011), smooth muscle cells and myofibroblasts (Heinrich *et al.* 2011), as well as Cx43 and Cx32 transfected cell lines (Cotrina *et al.* 1998) through diffusion-driven dye transfer. The application of FRAP in the islet to measure gap junction coupling has been reported; however, the measurement of intercellular diffusion was possible only upon the ectopic expression of Cx32 (Quesada *et al.* 2003). Cx36 is expressed in the native islet and predominantly couples β cells (Ravier *et al.* 2005; Benninger *et al.* 2008) and measurement of physiological endogenous Cx36 gap junction coupling was not possible, probably because only anionic dyes were used. Therefore, identifying an appropriate cationic dye should allow FRAP measurements to robustly quantify and spatially resolve physiological Cx36 gap junction coupling and its regulation within the islet.

In this study, the suitability of the cationic dye Rhodamine 123 (Rh123) was investigated for use in measuring Cx36 gap junction coupling in islets through FRAP. The distributions of coupling in wild-type islets and in islets from a heterozygous Cx36 knockout mouse were found to be highly heterogeneous, as has been previously suggested (Pipeleers 1992; Wojtusciszyn *et al.* 2008). Several modulators of Cx36 gap junctions were also tested through this technique. We finally confirmed that minimal to no Cx36 gap junction coupling is observed between α cells and β cells. This study has validated FRAP with Rh123 as a viable, non-invasive technique to quantify the distribution and regulation of Cx36 gap junction coupling in the islet with cellular resolution of coupling across the islet.

Methods

Ethical approval

All experiments involving mice were performed as per the institutional guidelines and appropriate laws, and were approved by the University of Colorado Institutional Animal Care and Use Committee. The authors have read and understood the policies and regulations of *The Journal of Physiology* as outlined by Drummond (2009) and ensured that all experiments complied with these regulations.

Animal care

All mice were housed in a temperature- and light-controlled facility under a 12 : 12 h LD cycle and were given access to food and water *ad libitum*. Cx36-LacZ knockout mice and GLU-Venus mice were generated as previously described (Degen *et al.* 2004; Reimann *et al.* 2008). Genotype was verified by an automated genotyping process at Transnetyx, Inc. (Cordova, TN, USA).

Islet isolation and culture

Mice were anaesthetized by I.P. injection of ketamine (80 mg kg^{-1}; Vedco, Inc., St Joseph, MO, USA) and xylazine (16 mg kg^{-1}; Vedco, Inc.) prior to being killed by exsanguination. Islets were isolated by collagenase injection into the pancreas through the common bile duct, the pancreas was harvested and digested, and islets were handpicked from the digest as previously described (Scharp *et al.* 1973; Koster *et al.* 2002) in 8–16 week-old C57BL/6NHsd (C57BL/6) mice or 12–48 week-old GLU-Venus C57BL/6 mice (Reimann *et al.* 2008). For all experiments, 26 Cx36-LacZ knockout mice (mixed genders), 15 C57BL/6Hsd mice (female) and four GLU-Venus mice (mixed gender) were used to complete this study. Islets were cultured in RPMI-1640 medium (Life Technologies, Inc., Austin, TX, USA) with 10% fetal bovine serum (FBS), 11 mM glucose, 100 units ml^{-1} penicillin, and 100 μg ml^{-1} streptomycin at 37°C under humidified 5% CO_2. The following treatments were applied to the islets: (i) 100 μM 3-isobutyl-1-methylxanthine (IBMX) with 50 μM forskolin (Sigma-Aldrich Corp., St Louis, MO, USA) was applied to the islets for 24 h prior to imaging to increase intracellular cyclic adenosine monophosphate (cAMP$_i$); (ii) 50 μM 18-α-glycyrrhetinic acid (α-GA) (Sigma-Aldrich Corp.) or 100 μM mebeverine (Sigma-Aldrich Corp.) was applied to islets for 1 h prior to and while imaging to decrease gap junction coupling; (iii) 50 μM modafinil (Sigma-Aldrich Corp.) was applied to islets for 1 h prior to imaging; (iv) 2 mM, 5 mM or 11 mM glucose was applied to islets for either 1 h or 24 h prior to imaging, and (v) 20 mM glucose was applied to islets for either 10 min or 24 h prior to imaging. All samples were cultured for a total of 48 h prior to imaging as this culture time has been used in previous studies (Rocheleau *et al.* 2006; Hodson *et al.* 2013) and has been shown not to affect islet electrical coupling (Zhang *et al.* 2003).

Fluorescence recovery after photobleaching

Isolated islets were plated in 35 mm Petri dishes with a 14 mm glass bottom (No. 1.5 coverglass) micro-well (MatTek Corp., Ashland, MA, USA) coated with BD Cell-Tak (BD Biosciences, Inc., San Jose, CA, USA) according to the manufacturer's instructions and cultured for 30 min in Hank's balanced salt solution (HBSS). Islets were then cultured in RPMI medium, described above, for 48 h before imaging. Islets were stained with either 12.5 μM Rh123 (Sigma-Aldrich Corp.) or 50 μM calcein AM (Invitrogen Corp., Carlsbad, CA, USA) for 30 min at 37°C. Islets were imaged in HBSS (5 mM glucose) at room temperature on an LSM 510 Meta confocal microscope (Carl Zeiss Microscopy, GmbH, Jena, Germany) with a 40× 1.2 NA water immersion objective.

For C57BL/6 islets, Rh123 (507 nm excitation maximum, 529 nm emission maximum) was excited with an Argon laser at 488 nm at 2.82 mW cm^{-2} and detected with the following beam splitters/filters: a 700/488 nm short-pass dichroic beam splitter; a 490 nm long-pass secondary beam splitter, and a 505 nm long-pass emission filter. Images were acquired every 15 s, with a scan time of 1.57 s per image and an image size of 512 × 512 pixels. The bleaching plane for each islet was set at two or three cell layers in from the bottom of the islet. Three images were acquired before photobleaching to establish baseline fluorescence intensity. A region of interest (RoI) was drawn around half the islet and this RoI was photobleached through excitation with the Argon laser at 488 nm and 316.05 mW cm^{-2} for 150 cycles, resulting in a bleaching time of 235.5 s (Fig. 1*A*). Further experiments in which bleaching area, power and time were varied were also performed; the levels of each parameter are indicated where applicable. Images were acquired in a z-stack, whereby two images above and below the bleaching area were taken, with a spacing of 4 μm between images.

For GLU-Venus islets, Rh123 and Venus were excited with an Argon laser at 488 nm with a 700/488 nm short-pass dichroic beam splitter at 6.36 mW cm^{-2} power. Multispectral detection from 489–586 nm in 11 nm increments was used to capture fluorescence intensity spectra. Images were acquired every 5 s, with a scan time of 0.98 s per image and an image size of 256 × 256 pixels. An RoI was drawn around half the islet. This RoI was photobleached through excitation with a Coherent Chameleon infra-red femto-second laser at 720 nm and 2 × 10^5 mW cm^{-2} power for 120 cycles, resulting in a bleaching time of 117.6 s. Images were acquired in a z-stack, whereby two images above and below the bleaching area were taken.

Image analysis

For analysis of dye diffusion after photobleaching, image processing and analysis of fluorescence intensity in an RoI were accomplished using ImageJ (National Institutes of Health, Bethesda, MD, USA). Fluorescence intensity values were averaged for either the entire bleached area or for individual cells in the photobleached area of each islet. Unless otherwise indicated, fluorescence intensity was determined only in the plane of photobleaching. In general, fluorescence intensity sharply decreased immediately after photobleaching and increased following an inverse exponential function, as shown in Fig. 1*B*. From the raw fluorescence intensity, values for initial fluorescence intensity (I_o), intensity immediately after photobleaching (I_p), and the steady state or final fluorescence intensity (I_∞) were derived. The inverse exponential recovery of fluorescence can be represented by eqn (1), where k is the recovery rate (Nathanson *et al.* 1999):

$$I(t) = (I_\infty - I_p)(1 - e^{-kt}) + I_p \qquad (1)$$

From these fluorescence intensity values, represented in Fig. 1*B*, the percentage recovery (eqn (2)) and fraction bleached (eqn (3)) were calculated to characterize the respective amounts of bleaching and recovery for each RoI (Lee *et al.* 2011):

$$\%\text{Recovery} = 100 \times \frac{I_\infty - I_p}{I_o - I_p} \qquad (2)$$

$$\text{Fraction Bleached} = \frac{I_o - I_p}{I_o} \qquad (3)$$

In order to calculate the recovery rate, the fluorescence intensity values as shown in Fig. 1*B* and intensity over time (I_t) were arranged following eqn (4):

$$(1 - F(t)) = \frac{I_t - I_p}{I_\infty - I_p} = -e^{-kt} \qquad (4)$$

When $[-\ln(1 - F(t))]$ is plotted *versus* [time], this generates a straight line with a slope equal to the recovery rate (k). This analysis was completed for all RoIs described in this study in which the fraction bleached was >0.10.

For GLU-Venus islets, spectral unmixing was required to separate the Rh123 and Venus spectra for fluorescence recovery analysis. Fluorescence intensity for each fluorophore was obtained by imaging Rh123-stained C57BL/6 islets or unstained GLU-Venus islets from 489–586 nm emission in 11 nm increments. These spectra were used to unmix the raw spectra from the Rh123-stained GLU-Venus islets using a least-square fitting approach, assuming a linear combination of contributing fluorophores, whereby the linear equations were solved with the singular value decomposition method (ZEN; Carl Zeiss Microscopy, GmbH) (Tsurui *et al.* 2000; Dickinson *et al.* 2001). The resulting images of Venus fluorescence identified α cells, and Rh123 fluorescence intensity in GLU-Venus islets was used to calculate fluorescence recovery kinetics in individual α cells and β cells, as described above.

Statistical analysis

Statistical analysis was performed using the average from individual mice. Unless otherwise stated, data represent the mean over three mice; error bars indicate the standard error of the mean (S.E.M.). Unless otherwise stated, statistical significance was determined using an analysis of variance (ANOVA) test with Tukey's *post hoc* analysis with $\alpha = 0.05$ to determine differences between conditions in a dataset. Linear correlation was determined using the Pearson correlation coefficient (ρ); the regression trend

line and 95% confidence intervals are presented for each dataset.

Results

FRAP of Rh123 robustly quantifies Cx36 gap junction coupling

To verify that fluorescence recovery correlates with Cx36 gap junction coupling, Cx36 knockout mice were used with 100% (Cx36$^{+/+}$), 50% (Cx36$^{+/-}$) and 0% (Cx36$^{-/-}$) Cx36 gene expression, which corresponds to, respectively, 100%, 54 ± 8% and 5 ± 2% conductance compared with wild-type mice (Ravier *et al.* 2005; Benninger *et al.* 2008). Fluorescence images and representative data show clear differences in recovery percentage and recovery rate with changes in coupling with Rh123 (Fig. 1*C* and *D*). Clear recovery was observed in wild-type Cx36$^{+/+}$ islets, but little to no recovery was observed in Cx36$^{-/-}$ islets. Cx36$^{+/+}$ islets stained with the anionic dye calcein AM showed limited diffusion of the dye into the centre of the islet and did not show any fluorescence recovery in comparison with Rh123-stained Cx36$^{+/+}$ islets (Fig. 1*C* and *E*). Recovery curves in Cx36$^{+/+}$ islets stained with calcein AM did not differ statistically from those in Cx36$^{-/-}$ islets stained with Rh123. On average, whereas the photobleached region recovered to ~87% of the initial fluorescence, the unbleached region decreased in fluorescence by ~6% from the initial fluorescence (Fig. 1*F*).

The average recovery rate and percentage recovery in Cx36$^{+/-}$ islets amounted to 45 ± 2% and 35 ± 2%, respectively, of those measured in Cx36$^{+/+}$ islets (Fig. 2*A* and *B*). Although no recovery rate could be calculated in Cx36$^{-/-}$ islets as a result of the lack of any measured recovery, the percentage recovery was significantly lower than in both the coupled islet conditions and not significantly greater than zero.

To ensure consistency in the technique, bleaching parameters were varied to study the effects on bleaching amount and recovery characteristics. Whereas the fraction bleached [see eqn (3)] was strongly positively correlated with bleaching time ($\rho = 0.73 \pm 0.18$) (Fig. 3*A*) and laser intensity ($\rho = 0.83 \pm 0.11$) (Fig. 3*B*) and weakly positively correlated with the percentage area of the islet bleached ($\rho = 0.58 \pm 0.26$) (Fig. 3*C*), no significant correlation between fraction bleached and recovery rate was observed ($\rho = 0.17 \pm 0.54$) (Fig. 3*D*).

Bleaching and recovery were also characterized for individual cells with respect to cell layer depth and distance from the bleaching plane, as well as islet size to ensure uniformity in the data (Fig. 4*A*, *E* and *I*). Variability in the fraction bleached appeared to show a small, but not significant, trend to increase moving towards the outer edge of the islet. However, no significant differences were

observed in the fraction bleached, percentage recovery or recovery rate with distance from the bleaching region (Fig. 4*A–D*). No significant differences were observed in bleaching or recovery characteristics with cell layer depth either above or below the bleaching plane (Fig. 4*E–H*). Similarly, neither islet size, as represented by the surface area of the plane selected for bleaching (Fig. 4*I–L*), nor the percentage of the islet area bleached (data not shown) showed a significant correlation with fraction bleached, the percentage of recovery or recovery rate. Finally, the decrease in fluorescence in the unbleached region did not differ significantly between cells adjacent to the bleaching area and cells elsewhere in the unbleached islet (data not shown).

These data confirm that FRAP represents a robust technique for the specific measurement of Cx36 gap junction coupling in the islet, and that FRAP measurements of coupling in islets from a Cx36 knockout mouse correlate with electrophysiological measurements previously reported (Ravier *et al.* 2005; Benninger *et al.* 2008).

FRAP reveals the distribution of Cx36 gap junction coupling within the islet

Given the robustness of FRAP measurements and the average spatial independence within the bleaching region, we next quantified the variability of the recovery rate between cells within an islet. The distribution of the recovery rate and the percentage recovery in individual cells in the bleaching plane were very heterogeneous for both Cx36$^{+/+}$ (Fig. 5*A* and *B*) and Cx36$^{+/-}$ (Fig. 5*C* and *D*) islets. Cx36$^{+/+}$ islets showed a skew to the distribution such that a small population (8.6%) of cells had very fast recovery rates (>0.012 s^{-1}, $>176\%$ of the mean rate), whereas the majority (80.9%) of the rest of the cells recovered at 0.004–0.009 s^{-1} or 59–132% of the mean rate. A Mann–Whitney *U* test revealed a significant difference in the median percentage recovery and recovery rate ($P < 0.001$, $\alpha = 0.05$), as well as a significant difference in the distribution of percentage recovery and recovery rate ($P < 0.001$, $\alpha = 0.05$) in cells from Cx36$^{+/+}$ islets compared with those from Cx36$^{+/-}$ islets.

In Cx36$^{+/-}$ islets, the recovery rate was also heterogeneous with a skew in the distribution (Fig. 5*D*). However, the coupling distribution was more confined and no cells showed a recovery rate of >0.007 s^{-1} or a percentage recovery of $>70\%$. The S.D. of the distribution normalized to the mean coupling was slightly reduced in Cx36$^{+/-}$ islets (0.40) compared with Cx36$^{+/+}$ islets (0.69). As a result, in Cx36$^{+/-}$ islets a significant proportion of cells showed very low coupling with a recovery rate of <0.002 s^{-1} (16.7%) or with a percentage recovery of $<20\%$ (45.5%).

In Cx36$^{-/-}$ islets, both the percentage recovery and recovery rate (Fig. 5*E* and *F*) were highly skewed towards zero. The recovery rate had a larger range of values than the percentage recovery because a small population of cells still showed small amounts of coupling of up to 0.01 s^{-1}. However, the median rate was zero as >50% of cells showed no recovery at all.

Therefore, Cx36 gap junction coupling across islets was found to be highly heterogeneous, with a substantial skew in the distribution giving rise to a small population
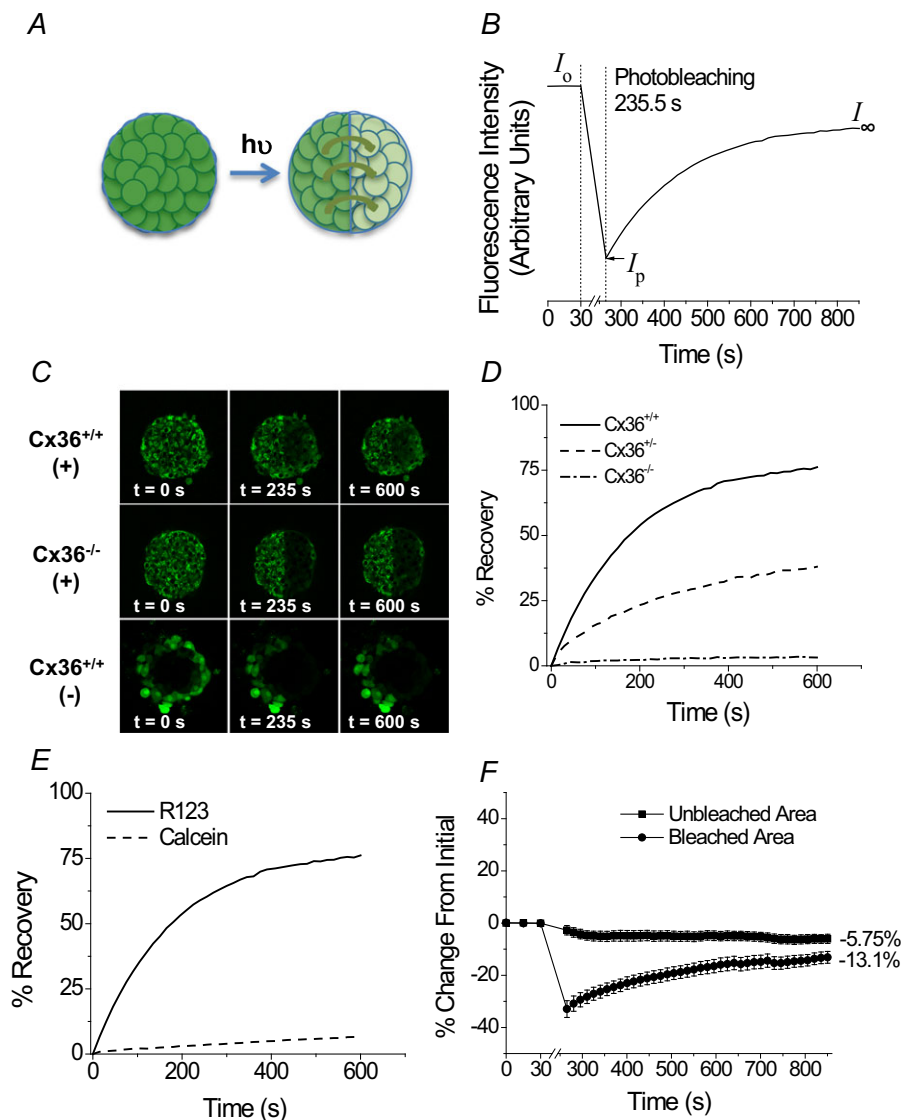
Figure 1. Fluorescence recovery after photobleaching (FRAP) with Rhodamine 123 (Rh123) measures diffusion across connexion36 (Cx36) gap junctions in the islet

A, schematic of FRAP experiments. Islets were stained with Rh123, half the islet was photobleached, and the diffusion of dye into the bleached region was quantified according to the intensity of fluorescence. *B*, representative data for fluorescence recovery as measured in the photobleached region of an islet, where Rh123 was photobleached for 235.5 s. Cx36 gap junction coupling is characterized by the kinetics of fluorescence recovery, where initial fluorescence (I_o), fluorescence immediately after photobleaching (I_p), and final fluorescence (I_∞) are used to calculate the amount of bleaching, percentage recovery and recovery rate. *C*, representative images of Rh123 fluorescence before photobleaching (0 s), immediately after photobleaching (235 s), and after fluorescence recovery (600 s) in Cx36 wild-type (Cx36$^{+/+}$) and homozygous knockout (Cx36$^{-/-}$) islets stained with Rh123 (+), as well as Cx36$^{+/+}$ islets stained with calcein AM (−). *D*, representative recovery curves for Cx36$^{+/+}$, heterozygous knockout Cx36$^{+/-}$ and homozygous knockout Cx36$^{-/-}$ islets. Data represent the mean ± s.e.m. over 10 islets (from three mice) for each time-point with the average final percentage change indicated for each condition. *E*, representative recovery curves for Cx36$^{+/+}$ islets stained with Rh123 or calcein AM. *F*, percentage change from the initial fluorescence intensity in the bleached or unbleached area of a Cx36$^{+/+}$ islet stained with Rh123.

of highly coupled cells or, upon reduced coupling, a population of negligibly coupled cells.

Modulation of functional Cx36 gap junction coupling measured with FRAP

To modulate Cx36 gap junction coupling and further test the accuracy of this technique, several treatments were applied to Cx36$^{+/+}$ islets to either increase or decrease gap junction coupling. The well-established gap junction inhibitor α-GA and recently identified inhibitor mebeverine reduced the percentage recovery to <50%

of the untreated islets; however, these values were still significantly higher than the percentage recovery and recovery rate in Cx36$^{-/-}$ islets (Fig. 6A).

Islets treated with the cognitive enhancer modafinil (Urbano *et al.* 2007) also enhanced the recovery rate by 1.3-fold above that of untreated controls (Fig. 6B). Treatment with forskolin and IBMX, to increase cAMP levels, increased the average percentage recovery by 1.7-fold (Fig. 6C) and the average recovery rate by 1.76-fold (data not shown). Cx36$^{-/-}$ islets treated with forskolin and IBMX showed little to no percentage recovery, similar to that of untreated Cx36$^{-/-}$ islets. Treatment with physiologically low (5 mM) and high
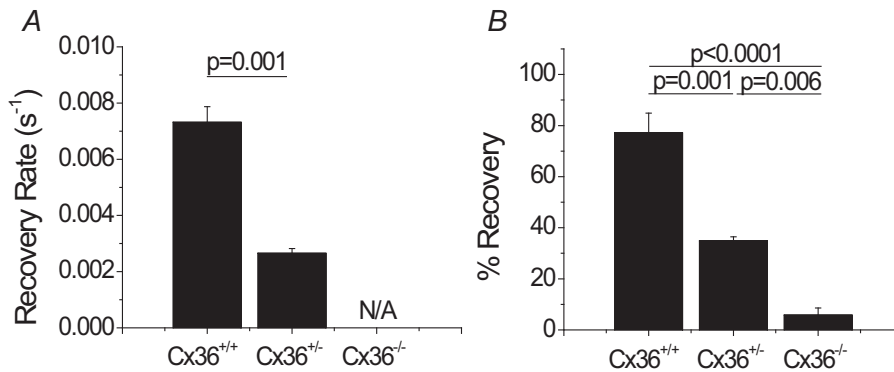

Figure 2. Specific levels of connexion36 (Cx36) gap junction coupling revealed using fluorescence recovery after photobleaching (FRAP)
Recovery rate (*A*) and percentage recovery (*B*) in Cx36$^{+/+}$, Cx36$^{+/-}$ and Cx36$^{-/-}$ islets as determined by analysis of FRAP data. Data are presented as the mean ± s.e.m. averaged over three or four mice per condition with two or three islets per mouse. N/A represents conditions at which recovery rates could not be calculated as a result of little or no fluorescence recovery.

Figure 3. Changes in bleaching time, laser power and the percentage of islet area bleached correlate with changes in fraction bleached, but fraction bleached does not affect recovery rate
Fraction decrease of total fluorescence intensity after photobleaching with respect to bleaching time (*A*), laser intensity (*B*), and percentage of the islet area bleached (*C*). *D*, fraction decrease of total fluorescence after photobleaching as a function of measured recovery rate. Each point represents the average fraction bleached over one or two islets from one mouse, where three mice were used per condition. The Pearson linear correlation coefficient (ρ) ± 95% confidence interval (95% CI) is displayed in the top right corner for each dataset. Linear regression trends and 95% CIs for the trends are also presented.
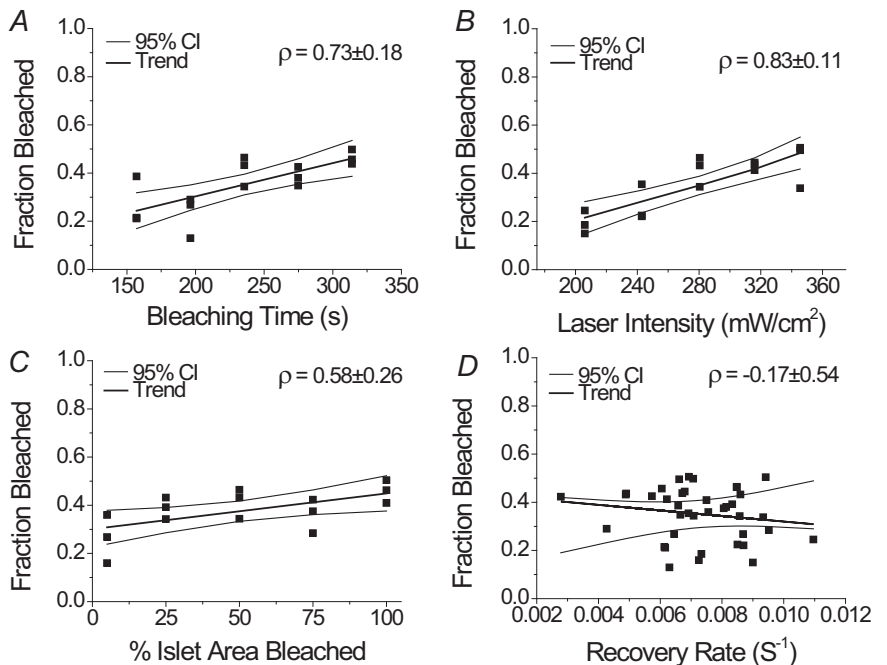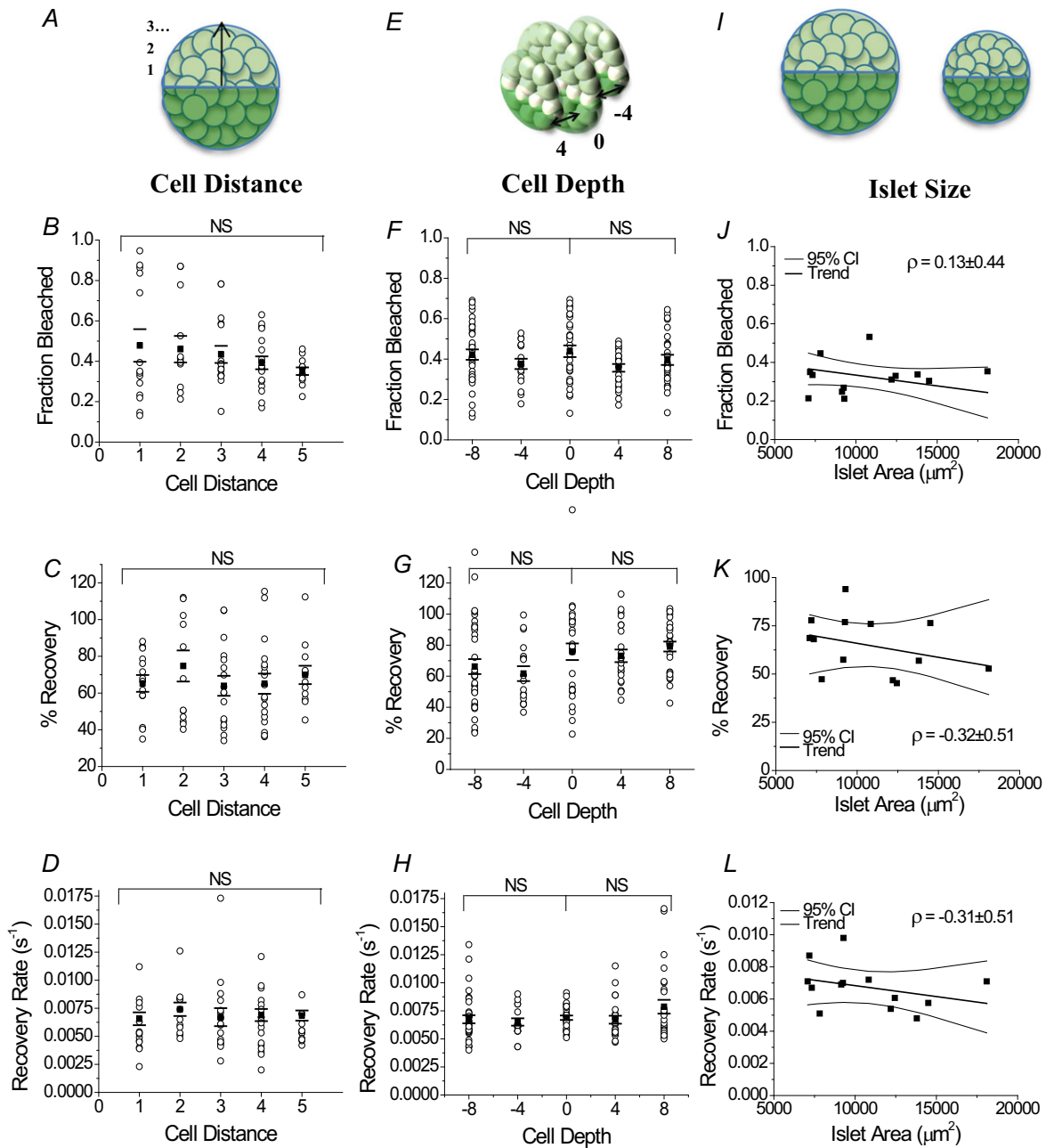
Figure 4. No differences emerged in fraction bleached and recovery characteristics with distance from bleaching area, depth above and below the bleaching plane, or islet area

Fraction decrease of total fluorescence intensity after photobleaching, percentage recovery and recovery rate as a function of cell layer distance from the centre edge of the bleaching plane (*A–D*) and as a function of cell layer depth above and below the bleaching plane (*E–H*). Data represent fluorescence recovery kinetics for individual cells (○), where the average over three mice (■) and s.e.m. (–) are presented for each cell layer, with each data point averaged over one or two islets per mouse. NS signifies no significant difference (*P* < 0.05) between conditions indicated in the brackets. *I–L*, fraction decrease of total fluorescence intensity, percentage recovery and recovery rate after photobleaching as a function of islet area, represented by the surface area of the plane selected for bleaching. Each point represents the average fraction bleached over 13 islets from three mice. The Pearson linear correlation coefficient (ρ) ± 95% confidence interval (95% CI) is displayed in the top right corner for each dataset. Linear regression trends and 95% CIs for the trends are also presented.

(11 mM) glucose concentrations revealed that both acute (Fig. 6D) and chronic (Fig. 6E) treatment with 11 mM glucose increased the recovery rate by >1.5-fold above the 2 mM baseline glucose treatment for the respective treatment times. Treatments of high glucose above physiological levels (20 mM) for different times differentially affected recovery rate (Fig. 6D and E): a 10 min treatment increased the recovery rate

two-fold and a 24 h treatment decreased the recovery rate by ~20% compared with the 2 mM baseline glucose treatment for the respective treatment times. These results confirm gap junction inhibitor action, together with a novel gap junction activator, and also identify $cAMP_i$- and glucose-dependent pathways for modulating Cx36 gap junction coupling in the islet.
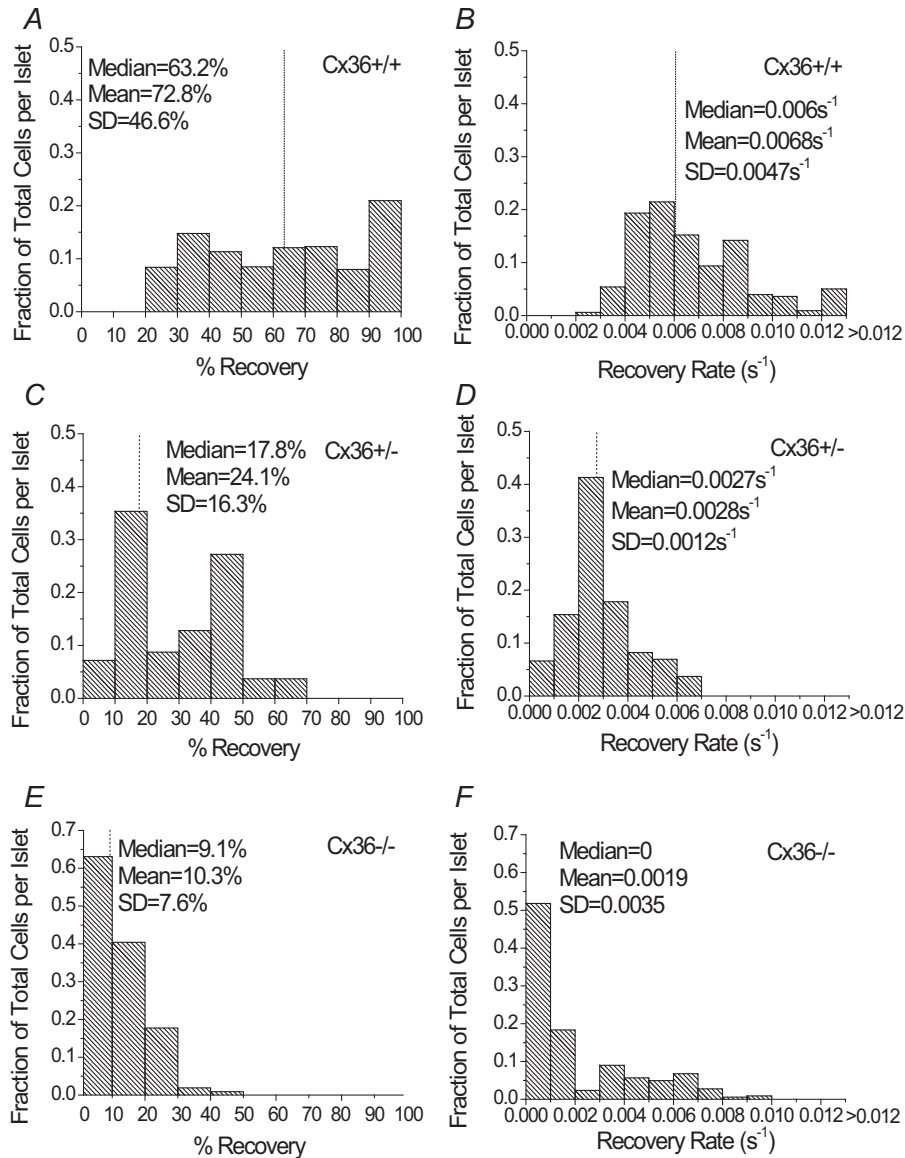

Figure 5. Fluorescence recovery after photobleaching (FRAP) reveals the distribution of recovery characteristics in connexion36 (Cx36)$^{+/+}$, Cx36$^{+/-}$ and Cx36$^{-/-}$ islets
Fraction of total cells per islet stained with Rh123, with a given percentage recovery in Cx36$^{+/+}$ islets (A), Cx36$^{+/-}$ islets (C) and Cx36$^{-/-}$ islets (E), and recovery rates in Cx36$^{+/+}$ islets (B), Cx36$^{+/-}$ islets (D) and Cx36$^{-/-}$ islets (F). Data represent the average fraction of total cells weighted over three mice, with data averaged over two islets per mouse for Cx36$^{+/+}$ mice and one or two islets per mouse for Cx36$^{+/-}$ mice, and one to three islets per mouse for Cx36$^{-/-}$ mice. The median, mean and s.d. of the percentage recovery or recovery rate over 173 cells for Cx36$^{+/+}$ mice, 48 cells for Cx36$^{+/-}$ mice and 116 cells for Cx36$^{-/-}$ mice are shown for cells from one or two islets per mouse with a total of three mice per coupling condition. The dotted line in each panel represents the location on the x-axis of the median value for each measurement.

FRAP confirms islet α cells and β cells are not functionally coupled by Cx36 gap junctions

To determine the extent of Cx36 gap junction coupling between α and β cells, we examined FRAP in islets with α cells labelled with the yellow fluorescent protein Venus. Linear unmixing was performed on raw images of Rh123 and Venus fluorescence over 489–586 nm and through photobleaching. Individual spectra for Rh123 and Venus showed maximum fluorescence intensity at 533 nm for Venus and 544 nm for Rh123 (data not shown). Using linear spectral unmixing, the raw image was separated into one image for each fluorophore, with a small unmixing residual image (Fig. 7A). Linear unmixing of the raw images provided separate fluorescence intensity

measurements for Rh123 and Venus fluorophores in both α cells and β cells, allowing for analysis of Rh123 recovery in both cell types. Essentially no recovery ($3.4 \pm 0.4\%$) was observed in α cells surrounded only by β cells. In contrast, β cells recovered to ~77% (Fig. 7B). The average percentage recovery in α cells over time was approximately zero (Fig. 7C) and a clear difference in the percentage recovery curve was observed between α and β cells. The recovery results for β cells in GLU-Venus islets are consistent with those in C57BL/6 islets, in which no significant difference in percentage recovery or recovery rate was observed (data not shown). Therefore, these results confirm that α and β cells within the islet are not functionally coupled by Cx36 gap junctions.
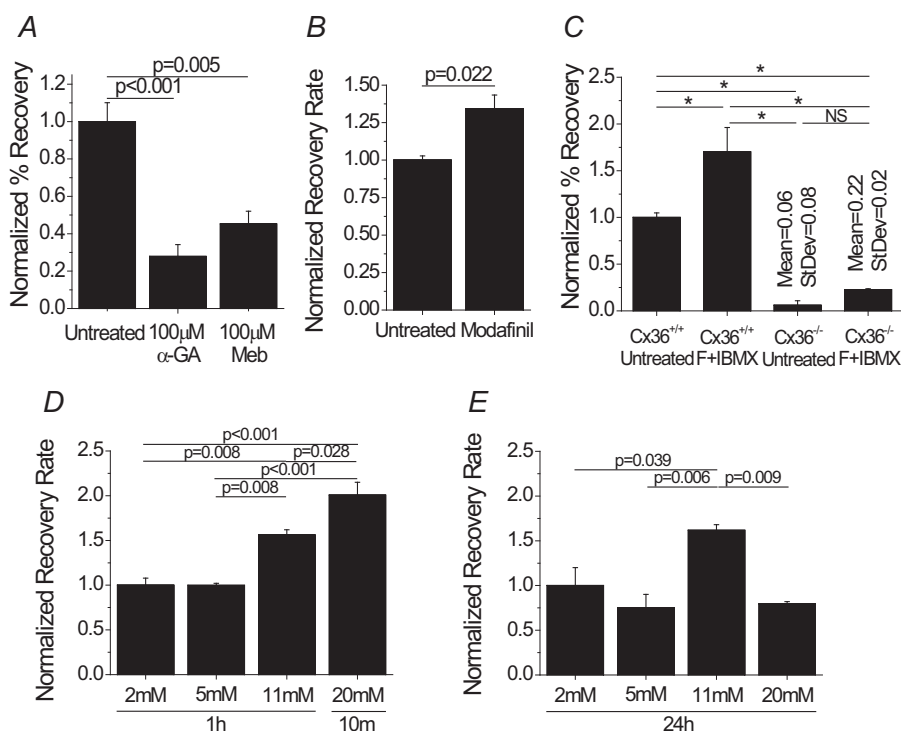

Figure 6. Fluorescence recovery after photobleaching (FRAP) quantification of modulation of connexion36 (Cx36) gap junction coupling
A, percentage recovery in islets treated with 100 μM 18-α-glycyrrhetinic acid (α-GA) or 100 μM mebeverine (Meb) normalized to untreated Cx36^{+/+} islets. Data represent the mean ± S.E.M. over three mice, with each data point averaged over one to three islets per mouse. *B*, recovery rate in Cx36^{+/+} islets either untreated or treated with 50 μM modafinil for 1 h, normalized to untreated islets. Data represent the mean ± S.E.M. over three mice, with each data point averaged over one to three islets per mouse. *C*, percentage recovery in Cx36^{+/+} and Cx36^{−/−} islets either untreated or treated with 100 μM 3-isobutyl-1-methylxanthine (IBMX) with 50 μM forskolin (F + IBMX) normalized to untreated Cx36^{+/+} islets. Data represent the mean ± S.E.M. over three or four mice, with each data point averaged over three or four islets per mouse. For Cx36^{−/−} islets, the mean and S.D. are also presented above the respective data columns. *D*, recovery rate in C57BL/6 islets cultured in 2 mM, 5 mM or 11 mM glucose for 1 h or 20 mM glucose for 10 min, normalized to recovery rate at 2 mM glucose. Data represent the mean ± S.E.M. over three mice, with each data point averaged over two or three islets per mouse. *E*, recovery rate in C57BL/6 islets cultured in 2 mM, 5 mM, 11 mM or 20 mM glucose for 24 h, normalized to recovery rate at 2 mM glucose. Data represent the mean ± S.E.M. over three mice, with each data point averaged over two to three islets per mouse. *P < 0.001. NS, no significant difference between conditions.

Discussion

Connexin36 gap junctions provide electrical coupling that is critical to the physiological function of the islet, and disruptions to Cx36 have been suggested to occur in early diabetes (Ravier *et al.* 2005; Carvalho *et al.* 2012; Head *et al.* 2012). However, no accurate and non-invasive technique that provides cellular resolution of coupling has yet been established to quantify these changes in the intact islet, and current techniques either assess a single peripheral cell or provide a static whole-islet average. The aim of this study was to establish FRAP using Rh123 as an accurate, non-invasive technique for quantifying Cx36 gap junction coupling in living islets. We have shown that this technique can accurately quantify specific levels of Cx36 gap junction coupling and have identified treatments that modulate gap junction coupling. This study has also confirmed that α cells and β cells do not form functional Cx36 gap junctions. This technique will enable future studies to examine changes in Cx36 gap junction coupling in the development of diabetes and uncover potential novel therapeutic targets associated with gap junction coupling.
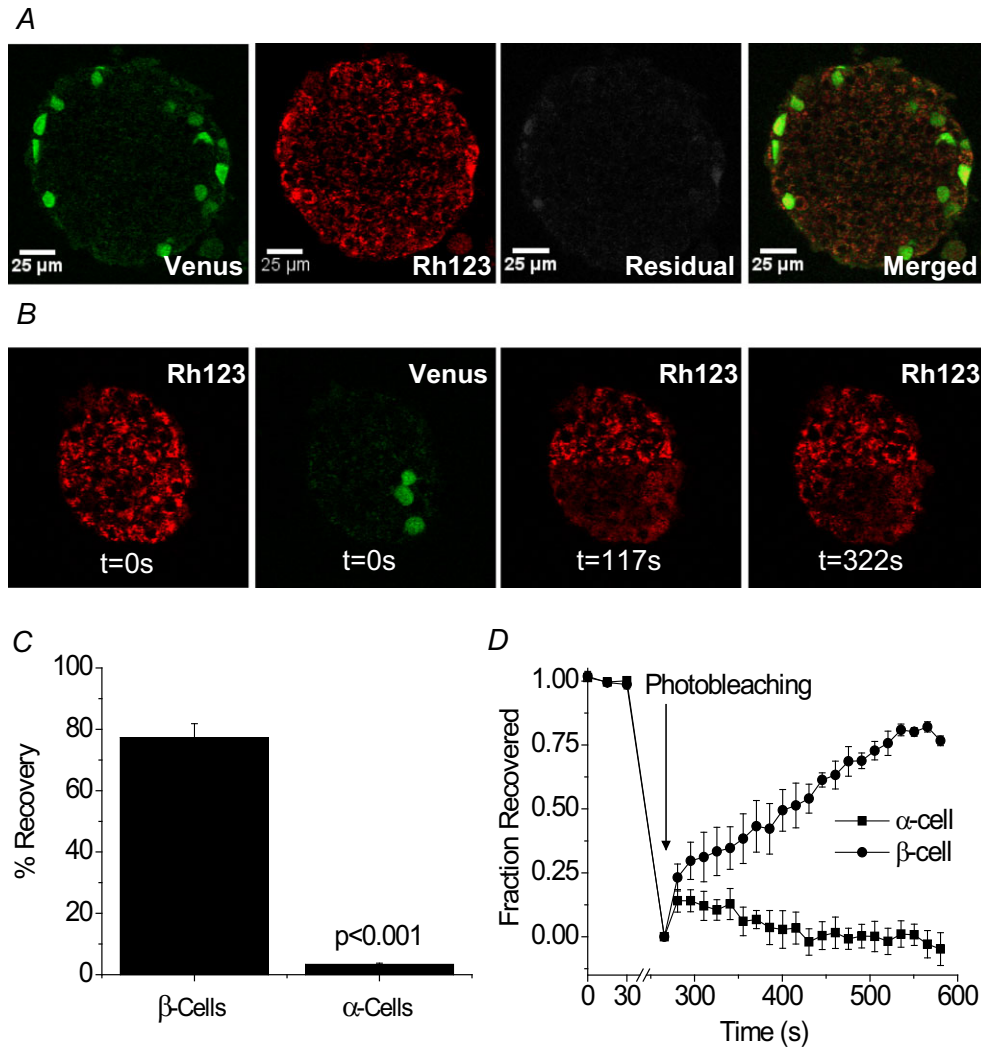

Figure 7. No functional connexion36 (Cx36) gap junction coupling between α cells and β cells in GLU-Venus islets

A, representative images of unmixed fluorescence for (left to right) Venus, Rhodamine 123 (Rh123), unmixing residuals and the merged final image. Spectra for Rh123 and Venus fluorophores were obtained from Rh123-stained C57BL/6 islets and unstained GLU-Venus islets, respectively. *B*, representative unmixed images of Rh123 before photobleaching (0 s), Venus expressing α cells before photobleaching, Rh123 immediately after photobleaching (117 s) and Rh123 after fluorescence recovery (322 s) in a GLU-Venus islet. *C*, percentage fluorescence recovery in α and β cells in a GLU-Venus islet. Data represent the mean ± s.e.m. over three mice, with each data point averaged over four to 24 cells from three to six islets per mouse. *D*, fraction of total fluorescence intensity recovered in α and β cells of a GLU-Venus islet. Data represent the mean ± s.e.m. fraction over three mice for each time-point, with each data point averaged over four to nine cells from three or four islets per mouse.

FRAP provides an accurate and robust method for quantifying Cx36 gap junction coupling in intact islets

In islets from mice with a knockout of Cx36 (Cx36$^{+/-}$, Cx36$^{-/-}$), which have defined decreases in electrical coupling, fluorescence recovery characteristics decreased in a similar manner to those in previous measurements of gap junction conductance (Benninger *et al.* 2008), indicating that the FRAP measurement scales approximately linearly with gap junction function. Both the recovery rate and recovery level (percentage) were in agreement, and each was independent of bleaching parameters and geometry, thereby allowing a robust assessment of coupling. The amount of photobleaching in Cx36$^{-/-}$ islets was greater than that in Cx36$^{+/+}$ islets, most likely as a result of dye diffusion during photobleaching in Cx36$^{+/+}$ islets. However, our control data (Fig. 3*D*) suggest that differences in bleaching amount should not affect recovery characteristics. In comparing FRAP measurements of gap junction coupling with cationic (Rh123) and anionic (calcein AM) dyes, our results showed a clear preference in Cx36 coupling for the cationic dye as calcein AM was unable to diffuse into the islet past the outer cell layer and displayed essentially no fluorescence recovery. This agrees with the findings of previous research, in which a similar preference of Cx36 for passing cationic molecules was observed (Charpentier *et al.* 2007).

When cells are loaded with Rh123, the diffusion across the plasma membrane is passive. However, the lack of recovery in islets from Cx36$^{-/-}$ mice indicates that diffusion across the plasma membrane between cells does not contribute significantly to the measured recovery rate. The fluorescence recovery rate measured with FRAP ($\sim$0.007 s^{-1}) was similar to that measured with LAMP in fibroblasts (0.0035–0.0125 s^{-1}) (Dakin *et al.* 2005); however, this rate is significantly lower than measurements of electrical coupling. This may limit the ability of this technique to measure fast changes in gap junction coupling, probably as a result of the difference in the rate of travel of electrical signals *versus* diffusion (Quesada *et al.* 2003; Ceriani & Mammano, 2013). However, the ability to spatially resolve changes in coupling represents a clear benefit in this study, as will be discussed.

The observed decrease in fluorescence intensity in the unbleached region of the islet indicates that dye is diffusing between cells in the islet. The observed final changes in fluorescence in the bleached and unbleached regions of the islet (Fig. 1*F*) differ, as has been reported elsewhere (Quesada *et al.* 2003; Heinrich *et al.* 2011). This may reflect non-uniform bleaching with increased depth into the islet, as has been demonstrated with one-photon bleaching of a plane in a three-dimensional object (Benninger & Piston, 2013). Dye diffusion from unbleached regions above and below the bleaching plane may therefore contribute to this difference.

Overall, the present data (Figs 1–4) and these considerations support FRAP as a viable and accurate technique to measure the endogenous Cx36-specific gap junction coupling in the mouse islet.

FRAP analysis on a cell-by-cell basis reveals heterogeneous coupling across the islet

FRAP was then used to characterize the spatial distribution of gap junction coupling in individual cells in the bleaching plane. A heterogeneous distribution of coupling was observed in islets from both a wild-type and a heterozygous Cx36 knockout mouse, similar to that observed in wild-type mouse β cell pairs (Moreno *et al.* 2005). Interestingly, in Cx36$^{+/+}$ islets, a small population of β cells appeared to be very highly coupled. Although heterogeneity has not been previously quantified in intact islets, this is consistent with recent studies examining $[Ca^{2+}]_i$ dynamics within the islet, which have implicated a small population of highly coupled cells that most efficiently mediate the synchronization of $[Ca^{2+}]_i$ dynamics across the islet (Stozer *et al.* 2013; Hraha *et al.* 2014). This is also consistent with the requirement of a heterogeneity of gap junction conductance to fully describe spatiotemporal $[Ca^{2+}]_i$ dynamics in mathematical models of the islet (Benninger *et al.* 2008; Goel & Mehta, 2013; Stozer *et al.* 2013; Hraha *et al.* 2014). Previous studies have reported high levels of electrical activity and insulin secretion in a small subset of β cells in the islet (Zhang *et al.* 2003; Wojtusciszyn *et al.* 2008; Benninger *et al.* 2011). Given that Cx36 gap junctions propagate electrical and $[Ca^{2+}]_i$ activity under high glucose and suppress electrical activity and depolarizing currents at low glucose (Rocheleau *et al.* 2006; Benninger *et al.* 2011), it is therefore appealing to consider whether Cx36 gap junction coupling correlates with electrical activity across the islet.

In Cx36$^{+/-}$ islets, some of the heterogeneity in coupling observed in wild-type islets was lost and the distribution of coupling with respect to the mean decreased. This arises from the loss of the small subset of highly coupled cells and the increase in a subset of very poorly coupled cells. Previous studies have shown alterations to Ca^{2+} oscillations (Ravier *et al.* 2005) and glucose tolerance (Head *et al.* 2012) in heterozygous Cx36 knockout mice. This similarly suggests this small subset of highly coupled cells is important in the physiological regulation of islet electrical activity.

In Cx36$^{-/-}$ islets, although the percentage recovery and recovery rate were mostly zero, a small population of cells that were still coupled was identified. Averaging over the entire bleached area masked this heterogeneity, which further demonstrates the utility of the spatial resolution of coupling using FRAP compared with other methods

that lack cellular resolution. Importantly, this may reveal another type of gap junction that provides very low-level coupling (see also below).

The ability of FRAP to spatially resolve cellular coupling with spatial resolution and to identify subpopulations of cells will allow future studies to correlate cell-specific function and cell coupling to further examine these roles.

Glucose- and cAMP$_i$-dependent modulation of Cx36 gap junction coupling

In an effort to modulate Cx36 gap junction coupling, several treatments that have previously been shown either to alter gap junction coupling in islets or to alter gap junction function or electrical coupling in other cell types were employed. Both α-GA and mebeverine are inhibitors of Cx36 gap junctions in the islet (Bertuzzi *et al.* 1999; Bavamian *et al.* 2012), and decreased gap junction coupling was observed through FRAP measurements in this study. However, not all coupling was abolished, which is consistent with the poor action and specificity of these inhibitors. Previous studies in hepatoma cells and cardiomyocytes have found that cAMP$_i$ can enhance gap junction trafficking to the plasma membrane (Paulson *et al.* 2000; Somekawa *et al.* 2005). Therefore, we investigated the effects of forskolin, a direct elevator of cAMP$_i$, and IBMX, a deterrent of cAMP$_i$ degradation, in modulating Cx36 gap junction coupling (Dachicourt *et al.* 1996). This treatment resulted in a specific increase in Cx36 gap junction coupling. Further study is needed to determine if this increase is a result of increased Cx36 trafficking and gap junction assembly, as in other cell types. Similarly, modafinil treatment resulted in an increase in Cx36 gap junction coupling. Modafinil is commonly used as a cognitive enhancer and has been shown to enhance neuronal electrical coupling, in which Cx36 is the main connexin forming gap junctions between neurons (Urbano *et al.* 2007). However, the mechanisms of action of modafinil in either islets or neurons are not well understood. Nevertheless, this treatment may point to a means of increasing gap junction coupling within the islet for therapeutic treatments.

In an effort to study changes in gap junction coupling with elevated glucose levels, we examined the impact of short (10 min to 1 h) and long (24 h) exposure periods. Physiologically elevated levels of glucose appeared to increase gap junction coupling, regardless of the duration of treatment, compared with lower glucose concentrations. The observed increase in gap junction coupling with a short period of hyperglycaemia is consistent with previous findings (Meda *et al.* 1979), and indicates a correlation between Cx36 gap junction coupling and glucose-stimulated electrical activity in the islet. By contrast, prolonged periods of hyperglycaemia

decreased gap junction coupling. This is consistent with studies in INS-1 cells, in which chronic treatment with 10 mM glucose maintained Cx36 mRNA levels, whereas treatment with 20 mM glucose decreased Cx36 mRNA over a 24 h culture period (Allagnat *et al.* 2005). This also suggests a potential role for Cx36 gap junction coupling in type 2 diabetes, in which persistent hyperglycaemia may lead to decreased coupling and impaired insulin secretion (Carvalho *et al.* 2012; Goel & Mehta, 2013).

Rh123 accumulation in the mitochondria is glucose-dependent. However, given the excess of dye in the cytoplasm, we do not anticipate that this would affect the dye transfer kinetics as the number and conductance of Cx36 gap junctions between cells is likely to represent the limiting factor for dye diffusion. This is supported by similar dye transfer rates upon varied amounts of photobleaching (Fig. 3).

In combination, these results indicate several means by which to achieve the modulation of Cx36 gap junction coupling, which may prove a useful target for treatments of type 2 diabetes. The FRAP approach presented here will allow for the robust investigation of the mechanisms that underlie these changes in Cx36 function.

Islet α and β cells do not form functional Cx36 gap junctions

The final aim of this study was to determine the extent of Cx36 gap junction coupling between α cells and β cells in the islet. It has been established that in response to glucose, both α and β cells exhibit oscillations in $[Ca^{2+}]_i$ and cAMP$_i$ (Marchand & Piston, 2010; Tian *et al.* 2011). Although these oscillations are near synchronous in α and β cells at elevated glucose, some differences in oscillations have been identified, making it unclear whether α and β cells are coupled by Cx36 gap junctions (Marchand & Piston, 2010). Although Cx36 has been reported to be expressed in low levels in α cells (Ito *et al.* 2012), the present data strongly indicate that functional Cx36 gap junctions do not form between α and β cells. However, other types of intercellular communication between these and other cell types may occur. Recently, evidence for the expression of Cx30.2, which forms voltage-gated gap junctions (Gemel *et al.* 2008), has been found and it is suggested that functional Cx30.2 gap junctions are formed in the islet (Coronel-Cruz *et al.* 2013). Results in Cx36$^{-/-}$ islets are consistent with this, although further study is needed to elucidate the role of these channels in islet function.

Conclusion

In summary, this study has outlined a new technique for the specific quantification of Cx36 gap junction coupling

throughout the islet, which provides for the cellular resolution of coupling. Using FRAP with the cationic dye Rh123, specific levels of gap junction coupling were identified and were found to match previous recordings of electrical conductance in islets with reduced or absent Cx36 expression or function. This technique was used to characterize the distribution of coupling across the islet in specific cell populations and to confirm the presence of a small population of highly coupled β cells in the islet. This technique can also be used to determine modulators of gap junction function, such as those tested in this study. Furthermore, the use of this technique confirmed that α and β cells in the islet do not form functional gap junctions. As changes in Cx36 gap junction coupling can have significant effects on the dynamics and regulation of $[Ca^{2+}]_i$ and insulin secretion, and are associated with the development of diabetes, this approach will be important to uncovering the underlying mechanisms of Cx36 regulation for potential therapies for diabetes.

References

Abbaci M, Barberi-Heyob M, Blondel W, Guillemin F & Dideldon J (2008). Advantages and limitations of commonly used methods to assay the molecular permeability of gap junctional intercellular communication. *BioTechniques* **45**, 33–62.

Allagnat F, Martin D, Condorelli DF, Waeber G & Haefliger J-A (2005). Glucose represses connexin36 in insulin-secreting cells. *J Cell Sci* **118**, 5335–5344.

Bavamian S, Pontes H, Cancela J, Charollais A, Startchik S, Ville DVD & Meda P (2012). The intercellular synchronization of Ca^{2+} oscillations evaluates Cx36-dependent coupling. *PLoS ONE* **7**, e41535.

Benninger RKP, Head WS, Zhang M, Satin LS & Piston DW (2011). Gap junctions and other mechanisms of cell–cell communication regulate basal insulin secretion in the pancreatic islet. *J Physiol* **589**, 5453–5466.

Benninger RKP & Piston DW (2013). Two-photon excitation microscopy for the study of living cells and tissues. *Curr Protoc Cell Biol* **4**, 1–24.

Benninger RKP, Zhang M, Head WS, Satin LS & Piston DW (2008). Gap junction coupling and calcium waves in the pancreatic islet. *Biophys J* **95**, 5048–5061.

Bertuzzi F, Davalli AM, Nano R, Socci C, Codazzi F, Fesce R, Carlo VD, Pozza G & Grohovaz F (1999). Mechanisms of coordination of Ca^{2+} signals in pancreatic islet cells. *Diabetes* **48**, 1971–1978.

Bukauskas F (2012). Neurons and β cells of the pancreas express connexin36, forming gap junction channels that exhibit strong cationic selectivity. *J Membr Biol* **245**, 243–253.

Carvalho CPF, Barbosa HCL, Britan A, Santos-Silva JCR, Boschero AC, Meda P & Collares-Buzato CB (2010). Beta cell coupling and connexin expression change during the functional maturation of rat pancreatic islets. *Diabetologia* **53**, 1428–1437.

Carvalho CPF, Oliviera RB, Britan A, Santos-Silva JCR, Boschero AC, Meda P & Collares-Buzato CB (2012). Impaired β cell–β cell coupling mediated by Cx36 gap junctions in prediabetic mice. *Am J Physiol Endocrinol Metab* **303**, E144–E151.

Ceriani F & Mammano F (2013). A rapid and sensitive assay of intercellular coupling by voltage imaging of gap junction networks. *Cell Commun Signal* **11**, 78.

Charpentier E, Cancela J & Meda P (2007). Beta cells preferentially exchange cationic molecules via connexin 36 gap junction channels. *Diabetologia* **50**, 2332–2341.

Coronel-Cruz C, Hernandez-Tellez B, Lopez-Vancell R, Lopez-Vidal Y, Berumen J, Castell A & Perez-Armendariz EM (2013). Connexin 30.2 is expressed in mouse pancreatic beta cells. *Biochem Biophys Res Commun* **438**, 772–777.

Cotrina ML, Lin JH-C, Alves-Rodrigues A, Liu S, Li J, Azmi-Ghadimi H, Kang J, Naus CCG & Nedergaard M (1998). Connexins regulate calcium signaling by controlling ATP release. *Proc Natl Acad Sci U S A* **95**, 15735–15740.

Dachicourt N, Serradas P, Giroix MH, Gangnerau MN & Portha B (1996). Decreased glucose-induced cAMP and insulin release in islets of diabetic rats: reversal by IBMX, glucagon, GIP. *Am J Physiol Endocrinol Metab* **271**, E725–E732.

Dakin K, Zhao Y & Li W-H (2005). LAMP, a new imaging assay of gap junctional communication unveils that Ca^{2+} influx inhibits coupling. *Nat Methods* **2**, 55–62.

Degen J, Meier C, van der Giessen RS, Söhl G, Petrasch-Parwez E, Urschel S, Dermietzel R, Schilling K, de Zeeuw CI & Willecke K (2004). Expression pattern of lacZ reporter gene representing connexin36 in transgenic mice. *J Comp Neurol* **473**, 511–525.

Dickinson ME, Bearman G, Tille S, Lansford R & Fraser SE (2001). Multi-spectral imaging and linear unmixing add a whole new dimension to laser scanning fluorescence microscopy. *BioImaging* **31**, 1272–1278.

Drummond GB (2009). Reporting ethical matters in *The Journal of Physiology*: standards and advice. *J Physiol* **587**, 713–719.

Farnsworth NL & Benninger RKP (2014). New insights into the role of connexins in pancreatic islet function and diabetes. *FEBS Letters* **588**, 1278–1287.

Gemel J, Lin X, Collins R, Veenstra RD & Beyer EC (2008). Cx30.2 can form heteromeric gap junction channels with other cardiac connexins. *Biochem Biophys Res Commun* **369**, 388–394.

Goel P & Mehta A (2013). Learning theories reveal loss of pancreatic electrical connectivity in diabetes as an adaptive response. *PLOS ONE* **8**, e70366.

Hauge-Evans AC, King AJ, Carmignac D, Richardson CC, Robinson IC, Low MJ, Christie MR, Persaud SJ & Jones PM (2009). Somatostatin secreted by islet δ cells fulfills multiple roles as a paracrine regulator of islet function. *Diabetes* **58**, 403–411.

Head WS, Orseth ML, Nunemaker CS, Satin LS, Piston DW & Benninger RKP (2012). Connexin-36 gap junctions regulate *in vivo* first- and second-phase insulin secretion dynamics and glucose tolerance in the conscious mouse. *Diabetes* **61**, 1700–1707.

Heinrich M, Oberbach A, Schliting N, Stolzenburg J-U & Neuhaus J (2011). Cytokine effects on gap junction communication and connexin expression in human bladder smooth muscle cells and suburothelial myofibroblasts. *PLoS One* **6**, e20792.

Hodson DJ, Mitchell RK, Bellomo EA, Sun G, Vinet L, Meda P, Li D, Li W-H, Bugliani M, Marchetti P, Bosco D, Piemonti L, Johnson P, Hughes SJ & Rutter GA (2013). Lipotoxicity disrupts incretin-regulated human *β* cell connectivity. *J Clin Invest* **123**, 4182–4194.

Hraha TH, Bernard AB, Nguyen LM, Anseth KS & Benninger RKP (2014). Dimensionality and size scaling of coordinated Ca^{2+} dynamics in MIN6 *β* cell clusters. *Biophys J* **106**, 299–309.

Ito A, Ichiyanagi N, Ikeda Y, Hagiyama M, Inoue T, Kimura KB, Sakurai MA, Hamaguchi K & Murakami Y (2012). Adhesion molecule CADM1 contributes to gap junctional communication among pancreatic islet *α* cells and prevents their excessive secretion of glucagon. *Islets* **4**, 49–55.

Koster JC, Remedi MS, Flagg TP, Johnson JD, Markova KP, Marshall BA & Nichols CG (2002). Hyperinsulinism induced by targeted suppression of *β* cell K$_{ATP}$ channels. *Proc Natl Acad Sci U S A* **99**, 16992–16997.

Lee J, Yim YS, Ko SJ, Kim DG & Kim CH (2011). Gap junctions contribute to astrocyte resistance against zinc toxicity. *Brain Res Bull* **86**, 314–318.

Marchand SJL & Piston DW (2010). Glucose Suppression of glucagon secretion: metabolic and calcium responses from *α* cells in intact mouse pancreatic islets. *J Biol Chem* **285**, 14389–14398.

Meda P, Perrelet A & Orci L (1979). Increase of gap junctions between pancreatic *β* cells during stimulation of insulin secretion. *J Cell Biol* **82**, 441–448.

Menge BA, Gruber L, Jorgensen SM, Deacon CF, Schmidt WE, Veldhuis JD, Holst JJ & Meier JJ (2011). Loss of inverse relationship between pulsatile insulin and glucagon secretion in patients with type 2 diabetes. *Diabetes* **60**, 2160–2168.

Moreno AP, Berthoud VM, Perez-Palacios G & Perez-Armendariz EM (2005). Biophysical evidence that connexin-36 forms functional gap junction channels between pancreatic mouse *β* cells. *Am J Physiol Endocrinol Metab* **288**, E948–E956.

Nathanson MH, Rios-Velez L, Burgstahler AD & Mennone A (1999). Communication via gap junctions modulates bile secretion in the isolated perfused rat liver. *Gastroenterology* **116**, 1176–1183.

O'Rahilly S, Turner RC & Matthews DR (1988). Impaired pulsatile secretion of insulin in relatives of patients with non-insulin-dependent diabetes. *New Engl J Med* **318**, 1225–1230.

Paulson AF, Lampe PD, Meyer RA, TenBroek E, Atkinson MM, Walseth TF & Johnson RG (2000). Cyclic AMP and LDL trigger a rapid enhancement in gap junction assembly through stimulation of connexin trafficking. *J Cell Sci* **113**, 3037–3049.

Perez-Armendariz EM (2013). Connexin36, a key element in pancreatic beta cell function. *Neuropharmacology*, 1–10.

Pipeleers D (1992). Heterogeneity in pancreatic *β* cell population. *Diabetes* **41**, 777–781.

Quesada I, Fuentes E, Andreu E, Meda P, Nadal A & Soria B (2003). On-line analysis of gap junctions reveals more efficient electrical than dye coupling between islet cells. *Am J Physiol Endocrinol Metab* **284**, E980–E987.

Ravier MA, Guldenagel M, Charollais A, Gjinovci A, Caille D, Sohl G, Wollheim CB, Willecke K, Henquin J-C & Meda P (2005). Loss of connexin36 channels alters *β* cell coupling, islet synchronization of glucose-induced Ca^{2+} and insulin oscillations, and basal insulin release. *Diabetes* **54**, 1798–1807.

Reimann F, Habib AM, Tolhurst G, Parker HE, Rogers GJ & Gribble FM (2008). Glucose sensing in L cells: a primary cell study. *Cell Metab* **8**, 532–539.

Rocheleau JV, Remedi MS, Granada B, Head WS, Koster JC, Nichols CG & Piston DW (2006). Critical role of gap junction coupled K$_{ATP}$ channel activity for regulated insulin secretion. *PLoS Biology* **4**, e26.

Scharp DW, Kemp CB, Knight MJ, Ballinge WF & Lacey PE (1973). Use of Ficoll in preparation of viable islets of Langerhans from rat pancreas. *Transplantation* **16**, 686–689.

Somekawa S, Fukuhara S, Nakaoka Y, Fujita H, Saito Y & Mochizuki N (2005). Enhanced functional gap junction neoformation by protein kinase A-dependent and Epac-dependent signals downstream of cAMP in cardiac myocytes. *Circ Res* **97**, 655–662.

Sorensen H, Winzell MS, Brand CL, Fosgerau K, Gelling RW, Nishimura E & Ahren B (2006). Glucagon receptor knockout mice display increased insulin sensitivity and impaired *β* cell function. *Diabetes* **55**, 3463–3469.

Spier S, Gjinovci A, Charollais A, Meda P & Rupnik M (2007). Cx36-mediated coupling reduces *β* cell heterogeneity, confines the stimulating glucose concentration range, and affects insulin release kinetics. *Diabetes* **56**, 1078–1086.

Stozer A, Gosak M, Dolensek J, Perc M, Marhl M, Rupnik MS & Korosak D (2013). Functional connectivity in islets of Langerhans from mouse pancreas tissue slices. *PLOS Comput Biol* **9**, e1002923.

Tian G, Sandler S, Gylfe E & Tengholm A (2011). Glucose- and hormone-induced cAMP oscillations in *α* and *β* cells within intact pancreatic islets. *Diabetes* **60**, 1535–1543.

Tsurui H, Nishimura H, Hattori S, Hirose S, Okumura K & Shirai T (2000). Seven-color fluorescence imaging of tissue samples based on Fourier spectroscopy and singular value decomposition. *J Histochem Cytochem* **48**, 653–662.

Urbano FJ, Leznik E & Llinas RR (2007). Modafinil enhances thalamocortical activity by increasing neuronal electrotonic coupling. *Proc Natl Acad Sci U S A* **104**, 12554–12559.

Wojtusciszyn A, Armanet M, Morel P, Berney T & Bosco D (2008). Insulin secretion from human beta cells is heterogeneous and dependent on cell-to-cell contacts. *Diabetologia* **51**, 1843–1852.

Zhang M, Goforth P, Bertram R, Sherman A & Satin L (2003). The Ca^{2+} dynamics of isolated mouse *β* cells and islets: implications for mathematical models. *Biophys J* **84**, 2852–2870.

Additional information

Competing interests

None declared.

Author contributions

N.L.F. designed the experiments, researched the data and wrote the manuscript; A.H. and M.P. researched the data; R.K.P.B. designed the experiments and edited the manuscript. All authors have read and approved this manuscript for publication.

Funding

Acknowledgements